Interfacial instabilities due to immiscible fluid displacement in circular and non-circular microchannels

Lu, Yu; Kovalchuk, Nina M.; Che, Zhizhao; Simmons, Mark J.h.

DOI:
10.1016/j.expthermflusci.2020.110045

Journal Pre-proofs

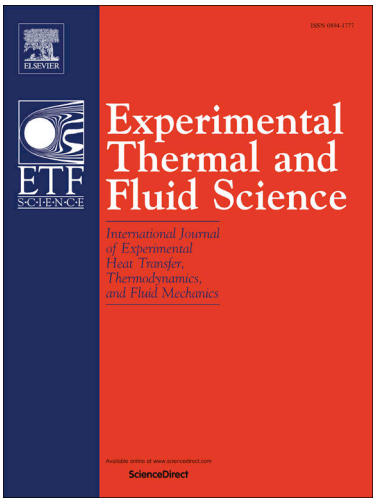

Interfacial instabilities due to immiscible fluid displacement in circular and non-circular microchannels

Yu Lu, Nina M. Kovalchuk, Zhizhao Che, Mark J.H. Simmons

PII: S0894-1777(19)31581-X
DOI: https://doi.org/10.1016/j.expthermflusci.2020.110045
Reference: ETF 110045

To appear in: *Experimental Thermal and Fluid Science*

Received Date: 20 September 2019
Revised Date: 6 January 2020
Accepted Date: 13 January 2020

Please cite this article as: Y. Lu, N.M. Kovalchuk, Z. Che, M.J.H. Simmons, Interfacial instabilities due to immiscible fluid displacement in circular and non-circular microchannels, *Experimental Thermal and Fluid Science* (2020), doi: https://doi.org/10.1016/j.expthermflusci.2020.110045

Interfacial instabilities due to immiscible fluid displacement in circular and non-circular microchannels

Yu Lu*[1], Nina M. Kovalchuk[1], Zhizhao Che[2], Mark J. H. Simmons[1]

[1]School of Chemical Engineering, University of Birmingham, Birmingham, B15 2TT, United Kingdom.

[2]Stage Key Laboratory of Engines, Tianjin University, Tianjin 300072, China.

Abstract

Interfacial instabilities caused by the displacement of one fluid by another were studied experimentally in three horizontal channels of different shape of cross section with hydraulic diameters ranging from 100 – 200 μm. Flow instabilities were induced by the displacement of a more viscous fluid (silicone oil) by an immiscible, less viscous fluid (aqueous solutions of glycerol) with viscosity ratios between the two fluids ranging from 20 to 100. In addition, the effect of surfactant was studied by the addition of Sodium Dodecyl Sulfate to the displacing fluid. Flow regime maps were developed for the different types of instability observed, with more complex 3-D instabilities shown to occur as the capillary number increases. Whilst fluid viscosities, channel shape and wall wettability were shown to affect the threshold capillary numbers for instabilities, the addition of SDS did not have a significant impact, which is believed to be a consequence of the long contact time between the two fluids during the whole displacement process. It was found that higher flow rates of the displacing fluid (resulting in more complex interfacial instabilities) did not cause a proportionally faster removal of the displaced fluid, which is an important finding for practitioners.

---

*Correspondence concerning this article should be addressed to Yu Lu at YXL413@alumni.bham.ac.uk

Keywords: Two-phase flow, microfluidic channel, instabilities, fluid displacement, surfactant, flow regime map.

1. Introduction

Microfluidic technology is attractive to both academia and industry due to the ability to closely control multiphase flow behaviour. As the channel diameter is reduced to O(10^{-4} – 10^{-3}) m or less, gravitational effects become insignificant and wall wettability and the interfacial properties of fluids become very important. Whilst much work has been done to understand the behaviour of two-phase flows in pipes of larger diameter, such as the work by Hewitt and Hall-Taylor (1970), Mandhane et al. (1974) and Weisman et al. (1979), the characterisation of flow patterns in microchannels has lagged until recently. The categorisation of the flow regimes and thus of the types of interfacial instabilities and development of flow regime maps are the main approaches taken: for example, Serizawa et al. (2002) characterised flow regimes for a 25 μm silica microchannel, with further studies classifying the types of interfacial instabilities observed.

Two phase flow by definition considers the concurrent transport of pairs of immiscible fluids. However, a related topic is the displacement of one immiscible fluid by another, the difference being that the fluid motion is caused by transport of the displacing fluid and its consequent entrainment of the previous fluid in the channel. Fluid displacement has an important role in industry both for manufacture e.g. the coating of capillaries, injection moulding, mechanical lubrication and ensuring hygiene (minimisation of contamination) in fluid changeover. Various geometries have been studied focussing on measurement of key features of the multiphase flow. For example, Lu et al. (2018) carried out measurements of residual film thickness in circular, square and near-semicircular cross sections; the data obtained showed good agreement with existing correlations. Scoffoni et al. (2001) studied the displacement of a more viscous fluid by a miscible, less viscous fluid flowing downwards in a vertical cylindrical 2 mm diameter tube. The viscosity ratio ranged from 10 to 400 in their experiments and they observed two different types of interfacial instabilities: termed axisymmetric and corkscrew modes, shown in Figure 1.

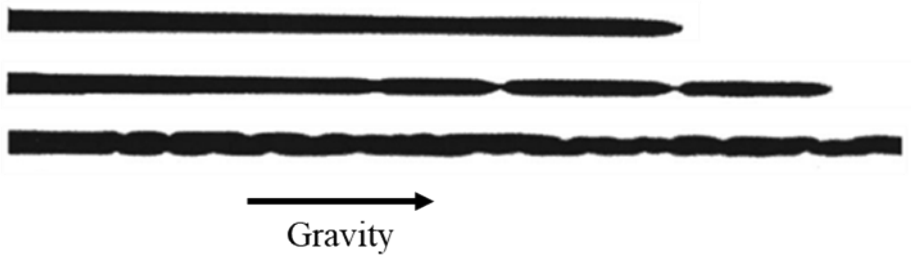

Figure 1 Instabilities from displacement experiment of a more viscous fluid by a less viscous miscible one in a vertical cylindrical tube: (from top to bottom) stable, axisymmetric mode and "corkscrew" mode. Figure reproduced from Scoffoni et al., 2001, with the permission of AIP Publishing.

Petitjeans and Maxworthy (1996) noted that fluid interfacial instabilities can sometimes cause an unfavourable mobility profile that leads to the reduction of the displacement efficiency. However, despite these experimental works and various 2-D and 3-D numerical studies of the fluid displacement process, for example using the Lattice Boltzmann method (Redapangu et al., 2012, 2013; Mishra et al., 2012; Swain et al., 2015), there are still a lack of systematic studies which examine interfacial topology/instability and velocity fields over a large range of critical parameters such as channel inclination, cross-sectional shape and fluid properties (density, interfacial tension, rheology). Some attempts have been made to develop diagrams showing the appearance of different types of unstable flows during fluid displacement (e.g. Scoffoni et al., 2001), but the effects of surface activity, (including dynamic interfacial tension effects) and wall wettability have not been studied in depth. Considering the potential application of channel cleaning, whether the appearance of flow interfacial instabilities can assist the clear-out of the pre-filled fluid also remains to be explored.

In this paper, a systematic study of the interfacial instabilities induced by the displacement of a more viscous fluid by a less viscous fluid with viscosity ratios from 20 to 100 is made in the same three horizontal channels used by Lu et al. (2018). From the interfacial instabilities observed, flow regime maps have been developed to reflect the influences of parameters such as the addition of surfactant, wall wettability, size and geometry of channel. A frame by frame image analysis method was used to

study the dynamics of the interfacial film, which provides insight into the removal efficiency of the displaced fluid.

2. Materials and methods

2.1 Microchannels

The microchannels used, identical to those used by Lu et al. (2018), had near-semicircular, circular and square cross-section. The near-semicircular channel used was the straight channel (Figure 2a) in a microfluidic chip from Dolomite® Microfluidics; the effect of wall wettability was studied using both hydrophilic and hydrophobic walls whilst keeping the geometry of the channel constant as shown in Figure 2a. Circular and square channels (Figure 2b), which contain the inner main channel inserted in the outer channel with the gap between the two filled with water, were made in-house. The schematics of the cross-section of these channels are shown in Figure 2c. Two sizes of circular channel were used, with diameters of 100 μm and 200 μm respectively. The detailed fabrication process for these two microchannel devices is described in Lu et al. (2018) and Table 1 lists the dimensions of the microchannels used.

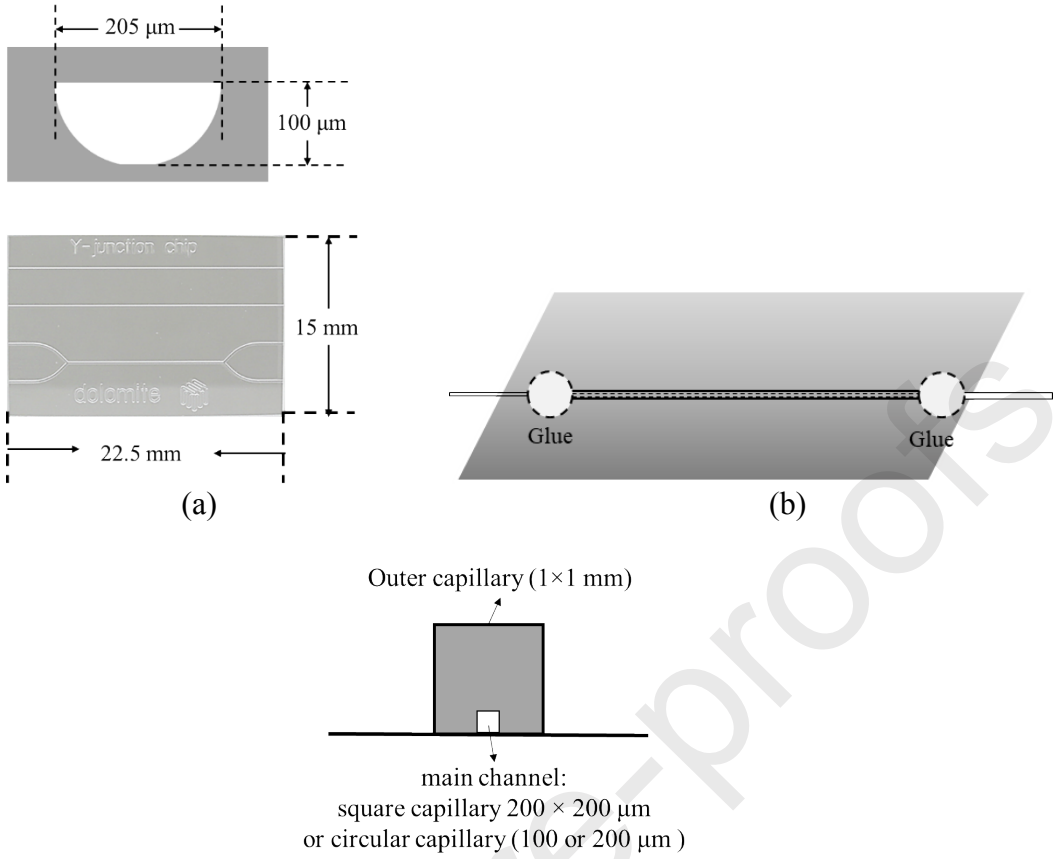

Figure 2 (a) Near semi-circular channel (the straight channels in the microfluidic chip from Dolomite); (b) Schematic of in-lab made device (circular and square channels); (c) schematic of the cross-section of the in-lab made channel. (Figures adapted from Lu et al., 2018, used under CC BY 4.0 Licence)

Table 1 Dimensions of microchannels used in this work

	Near-semicircular	Circular		Square
Size	205 µm width, 100 µm height	200 µm diameter	100 µm diameter	200×200 µm
Hydraulic diameter (µm)	124.6	200	100	200

2.2 Materials

In each experiment a pair of immiscible fluids is used. In this study, the fluid that is used to prefill the channel is referred to as *fluid 1* and the displacing fluid then injected is referred as *fluid 2*. Fluid pairs with different viscosity ratios ($\eta = v_1/v_2$, where v_1 and v_2 are the kinematic viscosities of fluid 1 and 2) were chosen, as shown in Table 2. Silicone oils were supplied by Sigma-Aldrich and 99.5% glycerol was supplied by ReAgent. A cationic surfactant, Sodium Dodecyl Sulfate (SDS, ReagentPlus® Sigma-Aldrich) was chosen to study the effect of interfacial tension on flow features. The concentration of SDS solution used was 4.7 g L^{-1}, which is twice the critical micelle concentration (CMC).

Table 2 Fluid pairs used in this study.

Fluid 1	*Fluid 2*	η
Silicone oil ($\nu_1=10^{-4}$ m^2 s^{-1})	Water	100
	Glycerol solution 1 (26.0% wt., $\nu_2=2\times10^{-6}$ m^2 s^{-1})	50
	Glycerol solution 2 (48.5% wt., $\nu_2=5\times10^{-6}$ m^2 s^{-1})	20
	Water + SDS	100
	Glycerol solution 1 + SDS ($\nu_2=2\times10^{-6}$ m^2 s^{-1})	50
	Glycerol solution 2 + SDS ($\nu_2=5\times10^{-6}$ m^2 s^{-1})	20
Silicone oil ($\nu_1=5\times10^{-5}$ m^2 s^{-1})	Water	50
	Glycerol solution 3 (32.6% wt., $\nu_2=2.5\times10^{-6}$ m^2 s^{-1})	20
Silicone oil ($\nu_1=2\times10^{-5}$ m^2 s^{-1})	Water	20

Equilibrium interfacial tension values, σ_s, were measured with the Wilhelmy plate method using a Krüss K100 tensiometer. Fluid 2 was dyed black with water-soluble Nigrosin (Sigma-Aldrich) for flow visualisation. The interfacial tension values between immiscible fluids are slightly affected by the dye (details can be found in Lu et al., 2018) and thus the interfacial tension values used in this study are the values obtained using *fluid 2* dyed with 10 g L^{-1} Nigrosin. Table 3 lists the equilibrium interfacial tension values for *fluid 2* dyed with Nigrosin (10 g L^{-1}).

Table 3. Equilibrium interfacial tension values between immiscible fluid pairs.

Fluid 1	*Fluid 2* (Contains Nigrosin 10 g L^{-1})	Equilibrium interfacial tension , σ_s, (mN m^{-1})
Silicone oil	Water	28
	Water + SDS	10
	Glycerol solutions	25
	Glycerol solutions + SDS	10

To evaluate the dynamic interfacial tension effects of the surfactant-laden *fluid 2*, dynamic surface tensions of *fluid 2* were first measured with maximum bubble pressure method using a SINTERFACE BPA-1S tensiometer. The dynamic interfacial tension was then estimated using the method proposed by Kovalchuk et al., (2018), using values of the surface tension of surfactant-free *fluid 2*, the equilibrium surface tension of surfactant-laden *fluid 2*, the interfacial tension between the *fluid 1* and surfactant-free *fluid 2* and the dynamic surface tension of surfactant-laden *fluid 2*. Details of the estimation method can be found in Lu et al., 2018.

2.3 Experimental procedure

The experimental setup is identical to that used in our previous work (Lu et al., 2018), a schematic of the setup is shown in Figure 3a. The microchannel device, placed horizontally on a microscope (Nikon

TE2000-s inverted microscope, 4× lens), is first filled with *fluid 1* through the inlet tubing, *fluid 2* needle is then connected to the inlet tubing ensuring no air goes into the tubing. The outlet of channel is vented to the atmosphere and the fluids drain into a waste beaker. *Fluid 2* is injected at desired flow rate in the range 5 – 3600 μL/min using a syringe pump (Harvard PHD 2000) equipped with a 5 mL or a 1 mL (for small flow rates) syringe (BD Plastipak). According to the manufacturer's specification the accuracy of the flow rate provided by the syringe pump is within ± 1%.

The experimental images were recorded at the desired channel position using a high-speed camera (Photron FASTCAM SA3) attached to the microscope. An external white colour cold light source MFO-90 (Microtec) was used to illuminate the channel from above and images were recorded through the objective lens facing upwards towards the channel. The imaging position was fixed at about 2/3 of the total channel length away from the channel inlet. This position was decided on the basis of the entrance length given by Shah and Bhatti (1987). For laminar flow, L_e = 0.06 *Re* D. Thus, L_e = 12.3 mm using the largest value of Re used in this study whilst still in laminar flow. For turbulent flow, $L_e = 1.359\ Re^{1/4}$, which gives a value of L_e = 7.6 mm from the largest overall value of Re. Figure 3b shows where images were typically recorded and an example image of *fluid 2* displacing *fluid 1*. The frame rates used were between 500 - 4000 f.p.s. with the exposure time set between 1 to 2×10^{-4} seconds.

(a)

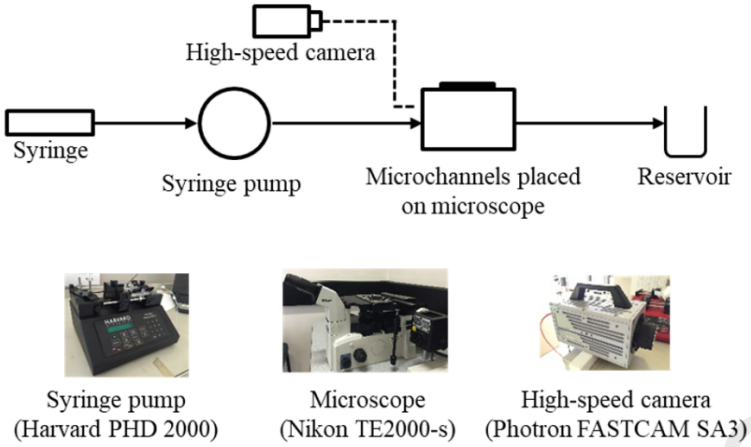

(b)

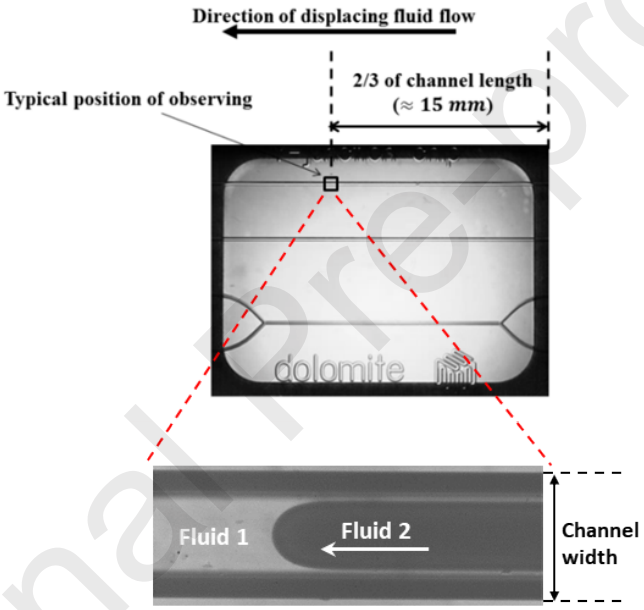

Figure 3 (a) Schematic of experimental set-up and pictures of some experimental equipment. (b) Typical position where images where recorded along the channel and an example of the recorded image in which fluid 2 enters the field of view

MATLAB codes were written to identify the interfaces between fluids 1 and 2 during fluid displacement, for which the strategy is shown in Figure 4. A line is first set at the position very close to the left end of the images (shown as a red line in the figure); then the grey scale values in each pixel are detected along this line across the width of the channel; the positions where maximum and

minimum in grey scale differences appear are recorded as the positions of the two interfaces. By repeating this process for each frame, the time evolution of the interfacial topology is revealed.

Figure 4 The position where the interfaces between fluid 1 and 2 is identified.

2.4 Dimensionless groups

The effect of interfacial tension, viscosity and injection flow rate are the important parameters considered in this study, capillary number was therefore chosen as the main characteristic dimensionless group. Depending on the viscosity used, two capillary numbers are used in this study, either:

$$Ca_1 = \frac{\mu_1 u}{\sigma} \tag{1}$$

or

$$Ca_2 = \frac{\mu_2 u}{\sigma} \tag{2}$$

Where μ_1 is the dynamic viscosity of *fluid 1*, μ_2 is the dynamic viscosity of *fluid 2*, u is the mean velocity of injected *fluid 2* and σ is the interfacial tension between *fluid 1* and 2. The *fluid 2* mean velocity, u, is calculated on the basis of the fluid travelling alone in the entire cross-section of the channel, i.e.

$$u = \frac{Q}{A_c} \tag{3}$$

Where Q is the injection flow rate of the *fluid 2* and A_c is the cross-section area of channel.

The uncertainty in the calculated values of capillary number depends on uncertainty of experimental parameters such as the liquid viscosity, flow rate, interfacial tension and the area of channel cross-section. As mentioned in subsection 2.3 the uncertainty in the flow rate provided by the syringe pump is ± 1 %. The experimental error in the measurement of equilibrium interfacial tension has not exceeded 0.5 mN/m, giving a relative error ± 5 % at smallest measured value of the interfacial tension of 10 mN/m (see Table 3). The uncertainty in the viscosity values is mostly due to the temperature variations during the experiments (± 2 °C). For silicone oils the change in viscosity is around 1 %/°C (Lorenz and Kandelbauer, 2014) and for glycerol solutions in water in the studied range of concentrations it is around 4 %/°C (Glycerine Producers' Association, 1963).

According to the manufacturer, for the Dolomite® Microfluidics chip the tolerance is 2 µm on the depth and 4 µm on the width, which gives a relative uncertainty for the area of 2.6 %. It is assumed that the same uncertainty is applicable for the other channels. Thus, the uncertainty for the capillary numbers used in this study $\Delta_{Ca} = \sqrt{\Delta_{\mu}^2 + \Delta_{Q}^2 + \Delta_{\sigma}^2 + \Delta_{Ac}^2}$ can be estimated as $\Delta_{Ca1} \sim 6$ % and $\Delta_{Ca2} \sim 7$ %.

3. Results and discussion

Different interfacial phenomena were observed depending upon the fluid pair used, *fluid 2* injection condition, channel geometry and the addition of surfactant. In general, the interface between *fluid 1* and *fluid 2* can be either stable, which appear in images as a straight line parallel to the channel wall, or unstable. The sections below describe how different flow regimes are defined depending on the interfacial phenomena, the characterisation of these interfacial phenomena against experimental variables and how different parameters influence the appearance of the flow regimes.

3.1 Identification of interfacial instabilities in experiment

Three regimes based on the types of instabilities observed during the displacement process are shown in Figure 5a. *Stable* regime is the flow regime when no oscillation or interfacial instabilities are observed at the interfaces between *fluid 1* and *fluid 2* at all times. *Axisymmetric unstable* regime

represents the flow behaviour of periodic and axisymmetric interfacial instability with the axis of symmetry being the streamline of channel along the flow direction. This instability results in an axisymmetric pinching of *fluid 2* which is observed at all times after its first appearance following the finger shape tip and a short period of stable interface. *Asymmetric unstable* regime represents complex and asymmetric interfacial instabilities taking place between the two fluids. This type of instability was observed after the brief occurrence of the axisymmetric unstable flows.

The three flow regimes proposed in this study and shown in Figure 5a are very similar to the unstable flows observed by Scoffoni et al. (2001) for displacement by a miscible fluid (Figure 1), which were believed to be caused by viscosity stratification. This may indicate that despite the difference in channel orientation and size, the fluid displacement using miscible and immiscible fluid pairs with similar viscosity ratios can result in very similar unstable flows. However, in the study by Scoffoni et al. (2001), an increase in the inlet flow rate causes the flow to destabilize into either axisymmetric or asymmetric corkscrew shapes. In some cases the "corkscrew" mode instability evolved from the axisymmetric instability and in some cases it appeared rapidly without observable axisymmetric unstable regions. In the present study, it was found that all asymmetric unstable flows evolved from axisymmetric instabilities. Note, the asymmetric unstable regime in this study may contain various flow patterns. Figure 5b shows other examples of the asymmetric instabilities observed using various fluid pairs and channel geometries. The fluids, flow condition and the channel used for these images are as follows (from top to bottom): *Fluid 1*: 10^{-4} m^2 s^{-1} silicone oil, *Fluid 2*: 5 $\times 10^{-6}$ m^2 s^{-1} glycerol solution+SDS, Ca_2 = 0.64, in near-semicircular channel; *Fluid 1*: 2×10^{-5} m^2 s^{-1} silicone, *Fluid 2*: Water+SDS, Ca_2 = 0.04, in near-semicircular channel; *Fluid 1*: 10^{-4} m^2 s^{-1}silicone oil, *Fluid 2*: water+SDS, $Ca_2 = 3.2\times10^{-2}$, in near-semicircular channel; *Fluid 1*: 10^{-4} m^2 s^{-1} silicone oil, *Fluid 2*: water, Ca_2 = 0.034, in 200 μm circular channel. The appearance of these patterns is highly time-dependent and may change from one experiment to another. Therefore, all these patterns have been categorised into the *asymmetric unstable* flow regime. In addition, the first two flow patterns shown

in Figure 5b, the sharp-cornered asymmetric instabilities, were taken from experiments performed with the addition of surfactant SDS in the displacing fluids, these were never observed in experiments carried out without surfactant.

(a)

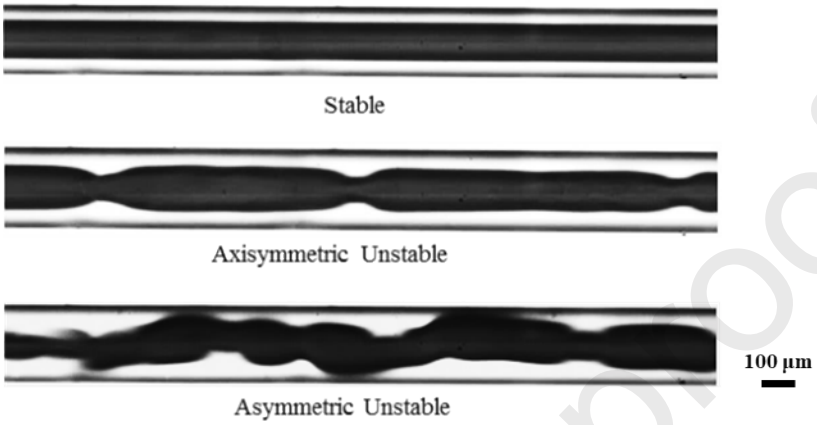

(b)

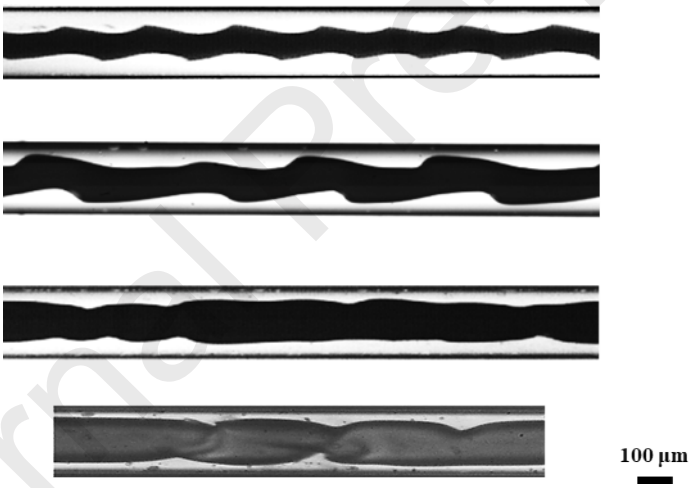

Figure 5 (a) Three flow regimes for immiscible fluid pairs, all three images are from the results of the displacement of 10^{-4} m^2 s^{-1} silicone oil by water in the near-semicircular channel using different injection flow rate: Stable ($Ca_2 = 9.8\times10^{-4}$), Axisymmetric Unstable ($Ca_2 = 9.7\times10^{-3}$) and Asymmetric Unstable ($Ca_2 = 1.9\times10^{-2}$). (b) Different types of Asymmetric interfacial instabilities observed in immiscible fluid displacement experiment. Fluids and flow conditions are described in the text.

3.2 Flow regime maps

Flow regime maps have been developed to relate the effects of injection flow rate, channel geometry, channel size, interfacial tension and channel wall properties upon the interfacial regime observed.

3.2.1 Effect of *fluid 2* viscosity

Figure 6 shows the flow regime maps obtained using three viscosities of *fluid 1* in the near-semicircular channel. These flow regime maps have been developed using the viscosity ratio of *fluid 1* to *fluid 2*, η, on the abscissa and capillary number on the ordinate, the latter reflecting the important role of interfacial tension. In each plot in Figure 6, the viscosity of *fluid 1* is fixed, therefore, the capillary number using the viscosity of *fluid 2*, Ca_2, is used here. Firstly, it can be observed from Figure 6a and 6b that by using a fixed viscosity of *fluid 1* and varying the viscosity of *fluid 2*, the transition capillary number between flow regimes decreases with the decrease of the viscosity of *fluid 2*.

The effect on transition conditions of the fluid pairs with the same viscosity ratios can be also seen from Figure 6. A viscosity ratio of 20 is achieved from three fluid pairs and viscosity ratio of 50 is achieved from two fluid pairs. There does not appear to be clear trend in behaviour at fixed viscosity ratio despite the use of non-dimensional parameters; hence the fluid viscosity of both phases has to be considered in the analysis.

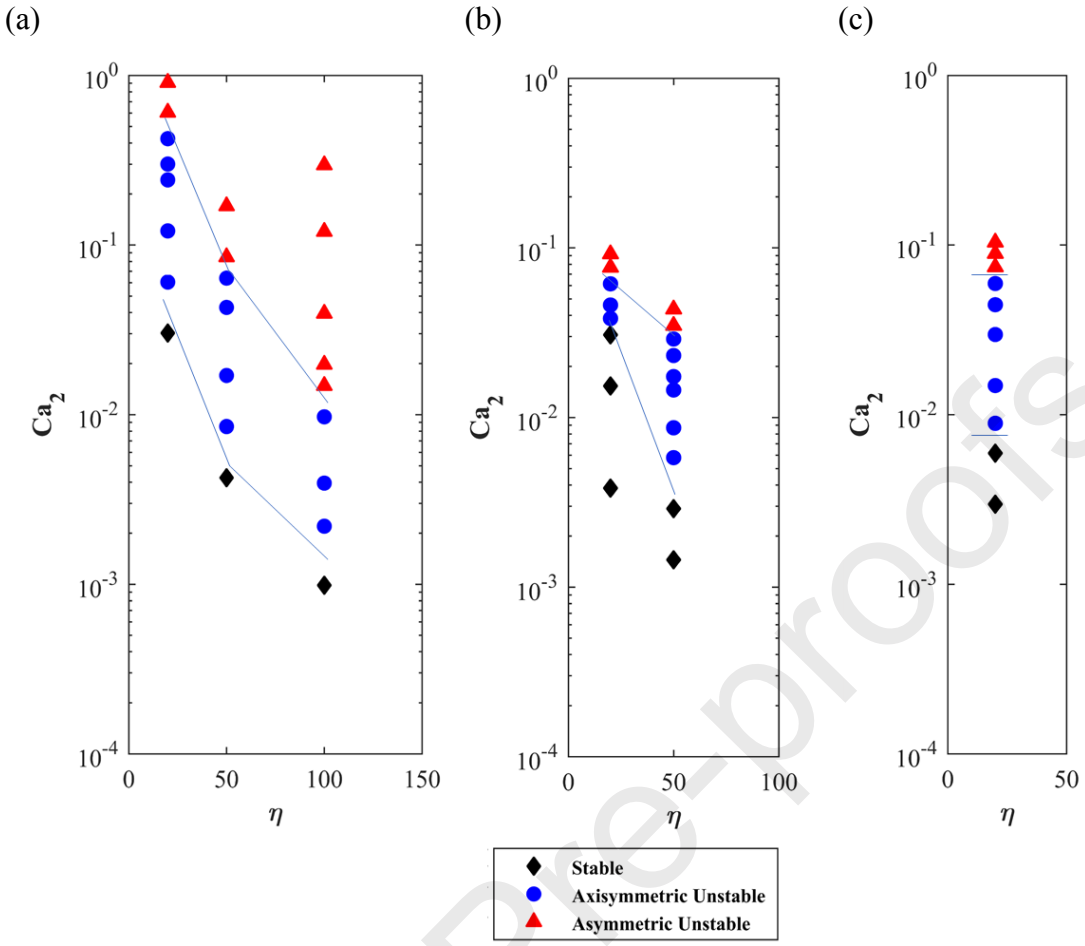

Figure 6 Flow regime map using (a) 10^{-4} m^2 s^{-1}, (b) 5×10^{-5}, (c) 2×10^{-5} m^2 s^{-1} silicone oil as *fluid 1*. In each plot, different viscosity ratios were achieved by varying the viscosity of *fluid 2*.

3.2.2 Effect of *fluid 1*

In order to see the influence of *fluid 1* on the appearance of interfacial instabilities, Figure 7a shows the results using a fixed *fluid 2* (water) but three viscosities of *fluid 1* (2×10^{-5}, 2×10^{-5} and 10^{-4} m^2 s^{-1} silicone oil). Together with the discussion above it is concluded that the decrease in *fluid 2* viscosity or the increase in *fluid 1* viscosity (whist keeping the viscosity of the other phase constant) results in a decrease in the regime transition capillary number Ca_2. It can be also concluded from Figure 2 that, for a given displacing *fluid 2*, an increase of viscosity of *fluid 1* results in a decrease of *fluid 2* velocity at the transition to instability.

The flow regime map reflecting the effect of the viscosity of *fluid 1* when the viscosity of *fluid 2* is fixed drives the development of a flow regime map using the capillary number based on fluid 1 viscosity, Ca_1, which is shown in Figure 7b.

It can be seen from Figure 7b that the transition condition between regimes, characterised by Ca_1, are very similar for different fluid 1 viscosities. It can therefore be hypothesised that when the viscosity of displacing fluid 2 is constant, for the conditions of viscosity ratio $20 \leq \eta \leq 100$, the transition conditions between three flow regimes are similar. However, the range of viscosities tested in this work is somewhat limited. The transition Ca_1 values between stable, axisymmetric unstable and asymmetric unstable flows are ~0.1 and ~1.

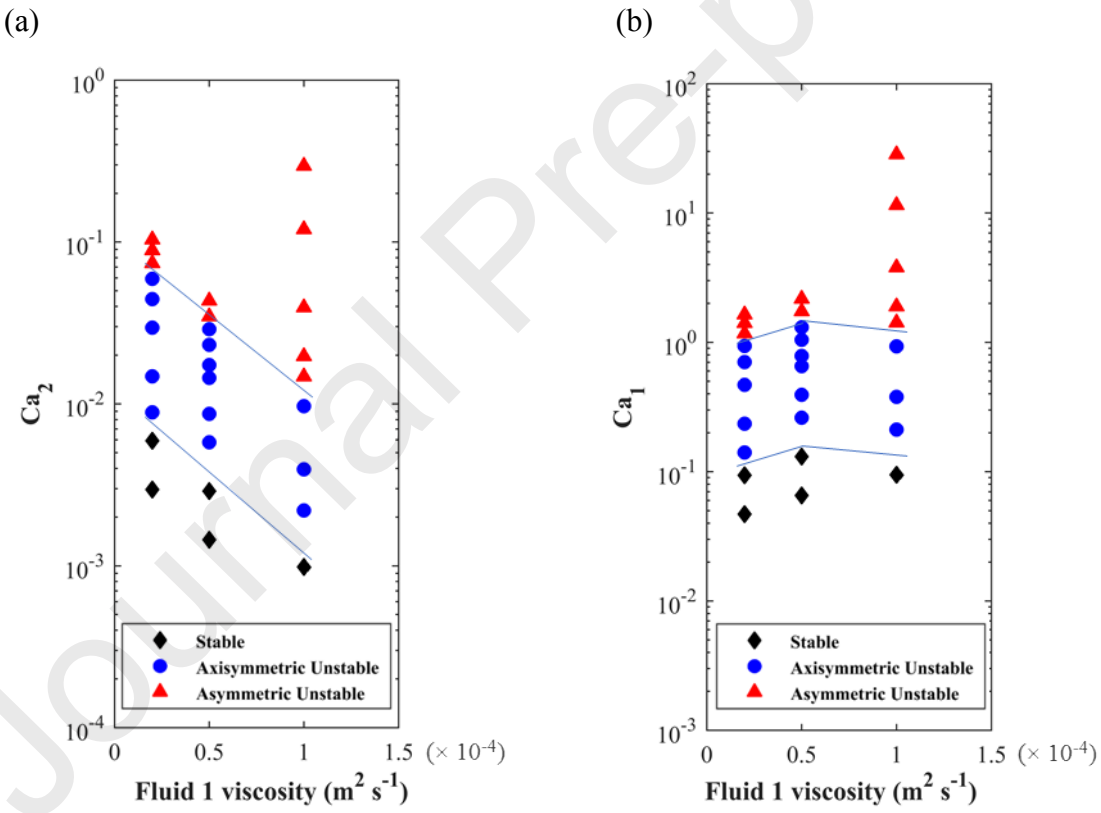

Figure 7 (a) flow regime map from the results using the fixed fluid 2 (water) and three viscosities of fluid 1, depending on Ca_2; (b) flow regime map reflecting the effect of fluid 1 viscosity with fixed fluid 2 viscosity, depending on Ca_1.

3.2.3 Surfactant-laden fluid 2

The comparison between the results using surfactant-free and surfactant-laden fluid 2 are shown in Figure 8. It is noted that by overlapping these two regime maps, the transition conditions for these two cases (based on Ca_2) are almost identical. Therefore, it can be concluded that for immiscible fluid displacement, by using the same fluid pairs, the effect of the addition of surfactant (in this case, a cationic surfactant SDS) in the displacing fluid can be expressed by the variation of equilibrium interfacial tension, which is reflected in the calculated values of capillary number. This suggests that dynamic interfacial tension does not play an important role given the timescales of adsorption at the interface for this surfactant and the timescales of the dynamics of this process. However, the addition of surfactant does cause morphological variations in the forms of asymmetric unstable flows, as shown in Figure 5, whose occurrence appears to be somewhat random.

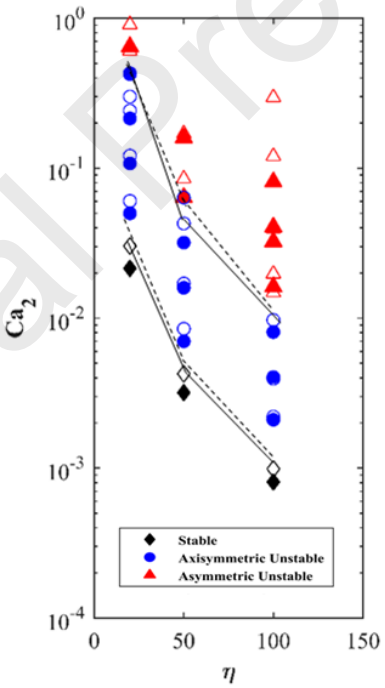

Figure 8 Comparison between flow regime maps of using surfactant-free (empty markers, dashed transition line) and surfactant-laden fluid 2 (solid markers, solid transition line). Silicone oil 10^{-4} m^2 s^{-1} was used as *fluid 1*, different viscosity ratios were achieved by varying the viscosity of *fluid 2*.

3.2.4 Effect of channel size and geometry

The effect of channel size was studied using two circular microchannels with diameters of 100 and 200 μm respectively, with identical fluid pairs and operating procedures being used for both. The overlapped flow regime map obtained is shown in Figure 9a, with the filled markers and solid lines representing the 200 μm channel.

It can be seen from Figure 9a that the values of capillary number at the transition between flow regimes for the 100 μm channel are shifted upwards from the 200 μm channel. This could be caused by the fact that the capillary number used here is calculated from the mean velocity of *fluid 2*, from the *fluid 2* injection flow rate and the cross-section area of the channel but the actual velocity of fluid 2 depends on the film thickness of fluid 1 left on the wall, which reduces the effective channel diameter and thus *fluid 2* travels faster. From previous work (Lu et al., 2018), the film thickness for 200 μm channel is generally larger than that for 100 μm channel, under similar flow conditions. Therefore, when Ca_2 values are the same, the real velocity of fluid 2 is higher in the 200 μm channel.

The flow regime maps using microchannels with the same hydraulic diameter (200 μm) but different cross-section shapes (circular and square) are shown in Figure 9b. It can be seen the change of channel geometry causes a significant shift in the transitions between flow regimes. Similar findings were reported for multiphase flows in small scale channels such as Sadatomi et al. (1982) and Coleman and Garimella (1999).

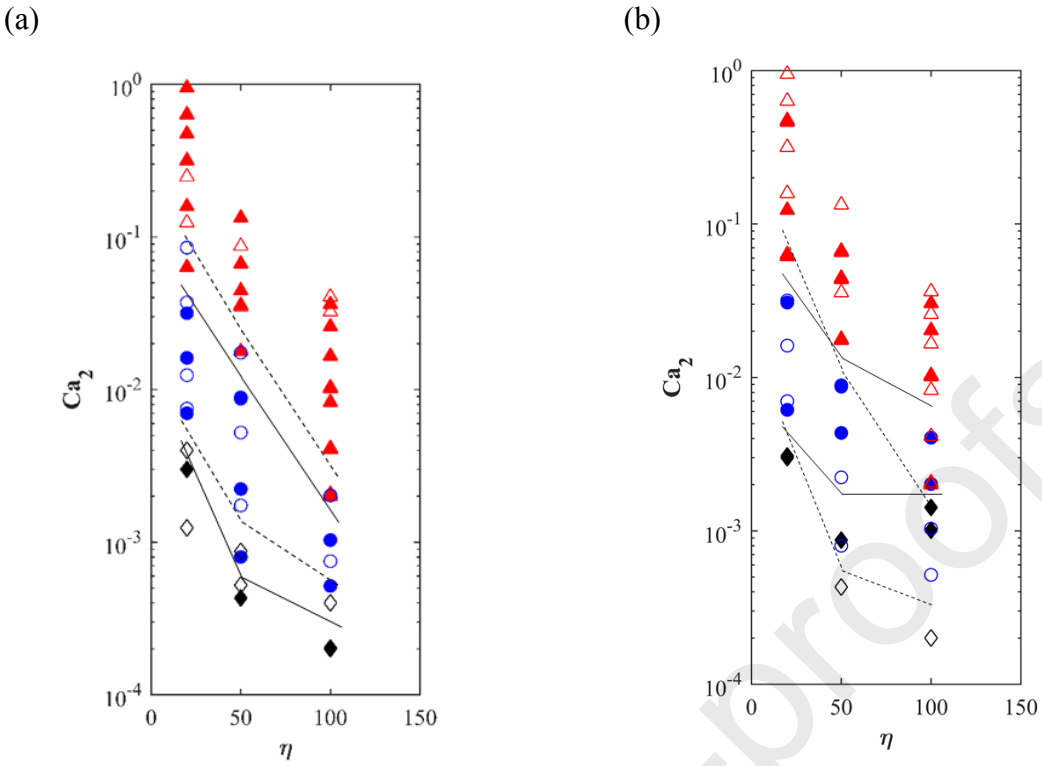

Figure 9 (a) Overlapped flow regime maps for the circular channels with 200 and 100 µm diameter. Filled markers and solid lines for 200 µm channel, empty markers and dashed lines are for 100 µm channel. (b) Overlapped flow regime maps using 200 × 200 µm square channel (coloured markers and solid line) and 200 µm circular channel (empty markers and dashed line).

3.2.5 Effect of wall wettability

To study the effect of wall wettability on the fluid displacement processes, near-semicircular channels of identical geometry but with hydrophobic or hydrophilic walls (Figure 2a) were used. Figure 10 shows the overlapped flow regime map obtained where solid markers and solid transition lines are for hydrophilic channel. From Figure 10 there exists a decrease in the transition capillary number for the hydrophobic channel. This differs from the findings in our previous work (Lu et al., 2018) which investigated the film thickness left on the wall. It was found that there was no significant difference between the film thickness left on wall for hydrophilic and hydrophobic channels. The fact that the

only place the aqueous phase (*fluid 1*) actually touches the wall is at the channel inlet, where *fluid 2* first contacts the channel wall, is believed to be the cause of this difference.

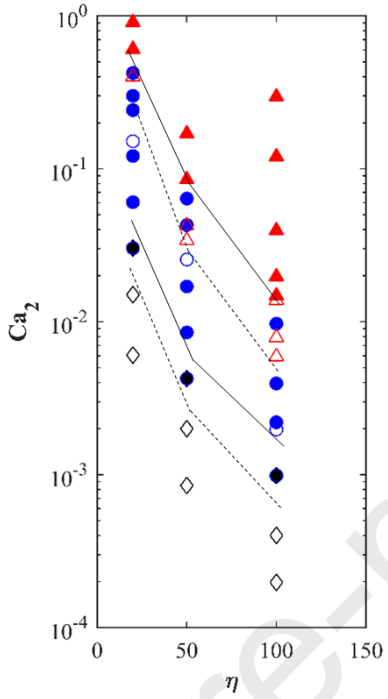

Figure 10 Overlapped flow regime maps for hydrophilic (solid markers and solid transition lines) and hydrophobic (empty markers and dashed transition lines) near-semicircular channel, using 10^{-4} m^2 s^{-1} silicone oil as *fluid 1*.

3.2.6 Interfacial film dynamics

Figure 11 shows an example of the evolution of the interface positions (red and blue curves) obtained using the MATLAB algorithm at a fixed spatial location of the channel marked with a red line in Figure 4. In order to show that this position chosen is representative of the flow patterns, the film thickness derived from the image processing results at this location is compared with another location as illustrated in Figure 12a. The flow condition was 10^{-4} m^2 s^{-1} silicone oil displaced by water in near-semicircular channel, $Ca_2 = 9.7 \times 10^{-3}$. Figure 12b shows the result of the film thickness at both positions 1 and 2. In both plots, time zero represents the frame just before the tip of *fluid 2* crosses the positions marked in Figure 12a. It can be seen that the flow features are equivalent at both positions. Position 1 was used for all further measurements.

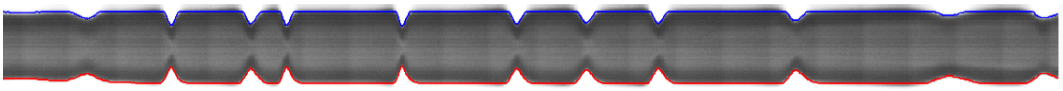

Figure 11 Temporal evolution of the interfaces. The video processed was from fluid displacement experiment of 1 × 10^{-4} m^2 s^{-1} silicone oil displaced by 5 × 10^{-6} m^2 s^{-1} glycerol solution in near-semicircular channel, Ca_2 = 0.54. 0.2 second of real time recording was processed in the shown image.

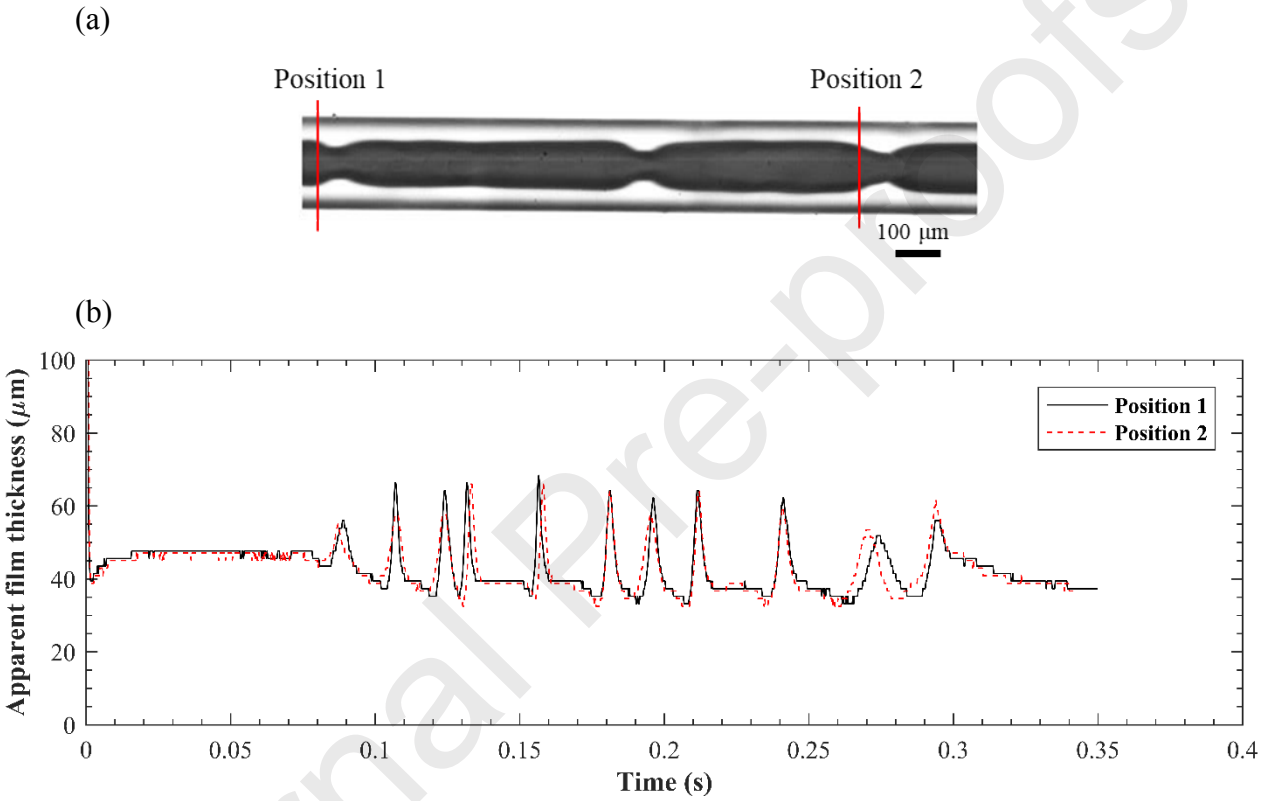

Figure 12 (a) The film thickness from Matlab image processing at position 1 and 2 are compared. (b) The film thickness on one side of channel at position 1 and 2. Flow condition: 10^{-4} m^2 s^{-1} silicone oil displaced by water, Ca_2 = 9.7 × 10^{-3}.

Figure 17a shows the film thickness derived from the image processing for the fluid pair of 10^{-4} m^2 s^{-1} silicone oil displaced by water in the near-semicircular channel at three different flow rates. The time axis shown in the figure starts from the first image processed, therefore time zero is the time just before fluid 2 enters the area of recording. Only the film thickness on one side (the top side in images) is shown because the flow is symmetric in the stable and axisymmetric unstable regimes. As shown in

Figure 17a, an initial sharp drop in film thickness can be seen due to the detection of the finger shape of the tip of fluid 2. In all three flow conditions, the plots then show a period of unchanged film thickness. This is in line with the previous definition of axisymmetric unstable flows, where axisymmetric instabilities take place after a short period of stable interfacial flows (explained in section 3.1). In addition, for the initial stable regimes, an increase in fluid injection flow rate (represented by Ca_2 here) results in higher film thickness. This is in good agreement with our previous work on the initial film thickness (Lu et al., 2018).

In Figure 13a, for flow conditions of $Ca_2 = 3.9\times10^{-3}$ and 9.7×10^{-3} in which axisymmetric instabilities were observed, the peaks of film thickness show the pinching parts of the unstable flows. When the capillary number increases, the extent of the shrinkage at the pinching parts of the flow increase. The average film thickness at the pinching parts is 62.3 μm for $Ca_2 = 9.7\times10^{-3}$ and 46.9 μm for $Ca_2 = 3.9\times10^{-3}$. The average frequency of the appearance of these pinching parts can also be estimated: 11 peaks appear for the higher capillary number flow with a period of 0.22 s, which corresponds to 50 Hz while for the flow of smaller capillary number condition, it is 35.7 Hz. The results shown in Figure 17a also suggest that the appearance of the peaks is not strictly periodic, meaning the time interval between the occurrence of each pinching event is not constant. The graph also shows that, under all flow conditions, the film thickness right after the tip shows a downwards peak. This means the width of fluid 2 experiences an initial expansion in width before shrinking back to form the stable non-wavy interface.

The film thicknesses for fluid pairs of 10^{-4} m^2 s^{-1} silicone oil displaced by 2×10^{-6} m^2 s^{-1} and 5×10^{-6} m^2 s^{-1} glycerol solutions are plotted in Figure 17b and c. The height of peaks representing the instabilities decreases over time, along with the decrease of the overall film thickness, represented by the baseline of the peaks. In addition, for most of the results shown in Figure 17b and c there exists the downwards peak before the initial stable flows.

It is clear from Figure 14 that at higher flow rates, unstable flow oscillations persist for a longer time, i.e. it takes longer for the interface to reach a condition which indicates the equilibrium state of the displacement process. This suggests that the occurrence of interfacial instabilities or the increase in the frequency resulting from higher injection flow rates, does not result in reaching the final equilibrium stage of the displacement process more quickly. It is assumed that the equilibrium state is achieved when there is no change of the interface between the two phases on the recorded images.

On the other hand, the final equilibrium value of the film thickness depends on injection flow rates and the viscosity ratios between the two fluids. Larger flow rates result in instabilities of larger amplitude leading to a larger difference between the initial and equilibrium film thicknesses. The relative effect increases with a decrease of viscosity ratio. When the viscosity ratio is large (Figure 15a, $\eta = 100$), the equilibrium film thickness is effectively independent of the flow rate. When a smaller viscosity ratio is used, as shown in Figure 16b or c ($\eta = 50$ or 20), the thinning caused by the instability can result in a smaller equilibrium film thickness under larger injection flow rate. However, even in the case of these smaller viscosity ratios, the dependence of the equilibrium film thickness of flow rate is rather weak, i.e. the increase in the flow rate of the displacing fluid does not provide the proportionally larger removal of liquid film.

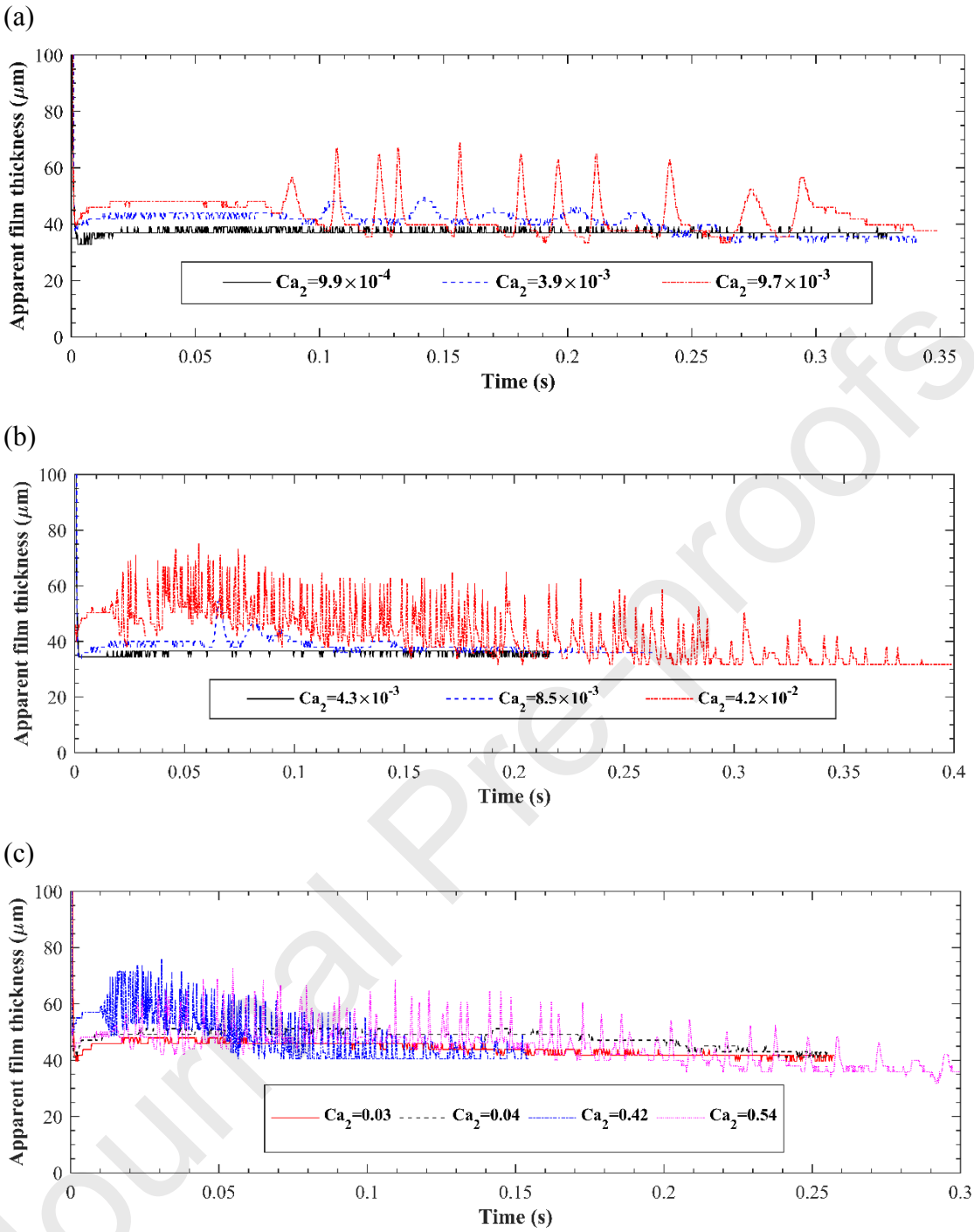

Figure 17 Film thickness for fluid pair of 10^{-4} m^2 s^{-1} silicone oil displaced by (a) water (η = 100), (b) 2×10^{-6} m^2 s^{-1} glycerol (η = 50) and (c) 5×10^{-6} m^2 s^{-1} glycerol solution (η = 20) in the near-semicircular channel. Three flow rates, represented by capillary numbers, are shown.

4. Conclusions

The interfacial phenomena obtained during immiscible fluid displacement in microchannels were studied. Immiscible fluid pairs with various viscosity ratios were used, together with the possible addition of a surfactant, SDS, in the displacing *fluid 2*.

The unstable flows were characterised by the type of interfacial instabilities observed from recorded images. Three flow regimes were categorised based on these interfacial instabilities and flow regime maps were developed to reflect the appearance of unstable flows under certain parameter settings.

It was found that by fixing the viscosity of one of the phases, the transition capillary numbers between flow regimes decrease as the viscosity ratio (expressed by the viscosity of displaced fluid over displacing fluid) increases.

By adding surfactant SDS into *fluid 2*, the flow regime map matches the map generated with surfactant-free *fluid 2* when the capillary number for surfactant-laden cases is calculated using the relevant equilibrium interfacial tension values. Thus, in this scenario, any effects due to dynamic interfacial tension are minimal, due to fast adsorption of surfactant to the interface over the timescale of the experiment.

A significant impact on the flow regime maps was observed for a change of channel size for channels of the same cross-sectional shape and a change of channel cross-section shape for channels with the same hydraulic diameter.

A hydrophobic treatment on the channel wall caused a shift of transitional capillary values in flow regime maps compared to the untreated channel, which is believed to be caused by the initial contact between the channel inlet and the displacing fluid.

Image processing revealed information such as the frequency of the appearance of the pinching parts of the axisymmetric unstable flows and gave some insights into the influences of injection flow rate and viscosity ratio on the removal of displaced fluid.

Acknowledgements

This research was funded by the EPSRC Programme Grant: "MEMPHIS – Multiscale Examination of Multiphase Physics in Flows" (EP/K003976/1). Yu Lu was funded by a PhD studentship from the School of Chemical Engineering, University of Birmingham.

Nomenclature

A_c	Channel cross-section area
Ca	Capillary number
D	Hydraulic diameter of channel
Le	Entrance length
Q	Fluid 2 injection flow rate
Re	Reynolds number
u	Displacing fluid mean velocity (based on A_c)
γ_s	Equilibrium surface tension
γ_{st}	Surface tension with surfactant at surface age t
η	Viscosity ratio (*Fluid 1*/*Fluid 2*)
γ_0	Surface tension without surfactant
μ	Dynamic viscosity
v	Kinematic viscosity
σ	Interfacial tension between two fluids
σ_s	Equilibrium interfacial tension
σ_{st}	Interfacial tension with surfactant at surface age t
σ_0	Interfacial tension without surfactant
Δ	Uncertainty

Reference

Al-Housseiny, T. T. and Tsai, P. A. and Stone, H. A., 2012. Control of interfacial instabilities using flow geometry. *Nature Physics*, 8, pp. 747-750.

Boomkamp, P. A. and Miesen, R. H., 1996. Classification of instabilities in parallel two-phase flow. *Engineering Fluid Dynamics,* 22(1), pp. 67-88.

Chung, P. M.-Y., Kawaji, M., Kawahara, A. and Shibata, Y., 2004. Two-phase flow through square and circular microchannels-Effects of Channel Geopmetry. *Journal of Fluids Engineering,* 126, pp. 546-552.

Coleman, J. W. and Garimella, S., 1999. Characterization of two!phase ~ow patterns in small diameter round and rectangular tubes. *International Journal of Heat and Mass transfer ,* 42, pp. 2869-2881.

Hassan, I., Vaillancourt, M. and Pehlivan, K., 2005. Two-phase Flow Regime Transitions in Microchannels: A Comparative Experimental Study. *Microscale Thermophysical Engineering,* 9, pp. 165-182.

Glycerine Producers' Association, 1963. *Physical Properties of Glycerine and Its solutions*. New York: Glycerine Producers' Association.

Hu, X. and Cubaud, T., 2016. Inertial destabilization of highly viscous microfluidic stratifications. *Physical Reviews Fluids*, 1, pp. 1-18.

Hewitt, G. F. and Hall-Taylor, N. S., 1970. *Annular two-phase flow.* 1st ed. ed. Oxford; New York: Pergamon Press.

Kovalchuk, N. et al., 2018. Effect of surfactant on emulsification in microchannels. *Chemical Engineering Science,* 176, pp. 139-152.

Lee, H. G. and Kim J., 2015. Two-dimensional Kelvin-Helmholtz instabilities of multi-component fluids. *European Journal of Mechanics B/Fluids*, 49, pp. 77-88.

Li, H. et al., 2014. Flow pattern map and time–frequency spectrum characteristics of nitrogen–water two-phase flow in small vertical upward noncircular channels. *Experimental Thermal and Fluid Science,* 54, pp. 47-60.

Lorenz, G. and Kandelbauer A., 2014. Silicones. In: H. Dodiuk and S. H. Goodman, ed. 2014. *Handbook of Thermoset Plastics*. Elsevier. Ch. 14.

Lu, Y., Kovalchuk, N. M. & Simmons, M. J. H., 2018. Residual film thickness following immiscible fluid displacement in noncircular microchannels at large capillary number. *AIChE Journal,* 64, pp. 3456-3466.

Malhotra, S. and Sharma, M. M., 2014. Impact of fluid elasticity on miscible viscous fingering. *Chemical Engineering Science*, 117, pp. 125-135.

Mandhane, J. M., Gregory, G. A. & Aziz, K., 1974. A flow pattern map for gas-liquid flow in horizontal pipes. *International Journal of Multiphase Flow,* 1(4), pp. 537-553.

Pamme, N., 2007. Continuous flow separation in microfluidioc devices. *Lab on a chip,* 7, pp. 1644-1659.

Sadatomi, M., Sato, Y. and Satuwatari, S., 1982. Two-phase flow in veritical noncircular channels. *International Journal of Multiphase Flow,* 8(6), pp. 641-655.

Scoffoni, J., Lajeunesse, E. & Homsy, G. M., 2001. Interfacial instabilities during displacement of two miscible fluids in a vertical pipe. *Physics of Fluids,* 13(3), pp. 553-556.

Serizawa, A., Feng, Z. and Kawara, Z., 2002. Two-phase flow in microchannels. *Experimental Thermal and Fluid Science,* 26, pp. 703-714.

Shah, R. K. and Bhatti, M. S., 1987. Laminar convective heat transfer in ducts. In: S. Kakac, R. K. Shah and W. Aung, eds. *Handbook of Single-Phase Convective Heat Transfer.* New York: Willy.

Weisman, J., Duncan, D., Gibson, J. & Grawford, T., 1979. Effects of fluid properties and pipe diameter on two-phase flow patterns in horizontal lines. *International Journal of Multiphase Flow,* 5, pp. 437-462.

Yu Lu: Formal analysis, Investigation, Data Curation, Writing – Original Draft, Visualization.

Nina M. Kovalchuk: Validation, Writing - Review & Editing.

Mark J. H. Simmons: Conceptualization, Methodology, Writing - Review & Editing, Supervision.

Zhizhao Che: Software.

The authors claim no conflict of interest.

• Interfacial instabilities were observed during fluid displacement in microchannels.

• The transition conditions of flow regimes are reflected in flow regime maps.

• Channel cross-section shape and size have significant impact on flow regime maps.

• The addition of surfactant did not bring significant variation to flow regime maps.

• High injection flowrate doesn't always help the clear-out of fluid being displaced.